

MIT Open Access Articles

Tunable impedance matching networks based on phase-switched impedance modulation

The MIT Faculty has made this article openly available. **Please share** how this access benefits you. Your story matters.

Citation: Jurkov, Alexander S., Aaron Radomski, and David J. Perreault. "Tunable impedance matching networks based on phase-switched impedance modulation." IEEE Energy Conversion Congress and Exposition, October 2017, Cincinnati, OH, USA, IEEE, 2017.

As Published: <http://dx.doi.org/10.1109/ecce.2017.8095887>

Publisher: IEEE

Persistent URL: <https://hdl.handle.net/1721.1/125221>

Version: Author's final manuscript: final author's manuscript post peer review, without publisher's formatting or copy editing

Terms of use: Creative Commons Attribution-Noncommercial-Share Alike



Tunable Impedance Matching Networks based on Phase-Switched Impedance Modulation

Alexander S. Jurkov
Massachusetts Institute of
Technology
Cambridge, MA

Aaron Radomski
MKS Instruments, Inc.
Rochester, NY

David J. Perreault
Massachusetts Institute of
Technology
Cambridge, MA

Abstract—The ability to provide accurate, rapid and dynamically-controlled impedance matching offers significant advantages to a wide range of present and emerging radio-frequency (RF) power applications. This work develops a new type of tunable impedance matching networks (TMN) that enables a combination of much faster and more accurate impedance matching than is available with conventional techniques. This implementation is based on a narrow-band technique, termed here *phase-switched impedance modulation* (PSIM), which entails the switching of passive elements at the RF operating frequency, effectively modulating their impedances. The proposed approach provides absorption of device parasitics and zero-voltage switching (ZVS) of the active devices, and we introduce control techniques that enable ZVS operation to be maintained across operating conditions. A prototype PSIM-based TMN is developed that provides a 50 Ohms match over a load impedance range suitable for inductively-coupled plasma processes. The prototype TMN operates at frequencies centered around 13.56 MHz at input RF power levels of up to 150 W.

I. INTRODUCTION

Dynamic component tuning and impedance matching have application to a diverse range of radio-frequency (RF) power applications, including software-defined radios [1], frequency-agile and adaptive RF transmitters and receivers [2], [3], the design of new types of highly-efficient RF power amplifiers [4], plasma drivers [17], generators [5], [6], wireless power transfer [7, 19], and power converters [14]. Electronically-controlled tunable impedance matching networks (TMNs) in particular can be valuable in many RF applications. Such TMNs typically match a variable load impedance to a desired input impedance (e.g., 50 Ohms) at an RF operating frequency (e.g., [15]), though other functions are possible.

For high-frequency (HF) and very-high-frequency (VHF) applications (e.g., 3-300 MHz), a TMN is typically implemented as an ideally-lossless, lumped-element reactive network, where some of its reactive elements are realized as variable (tunable) components. That is, the impedance of the tunable components at a particular frequency, or over a range of frequencies, can be controlled externally to dynamically match the load impedance to a desired input impedance. Based on the technology employed for realizing the variable reactance elements, conventional TMNs can be classified as either analog (continuously adjustable) or digital (adjustable among a set of discrete values). (Here we characterize the tuning mechanism itself, neglecting the fine-scale discretization that may be imposed by the control system.) The former group of TMNs relies on variable reactance elements whose value (at some

frequency or over a range of frequencies) can be tuned in an (ideally) continuous manner. For instance, conventional high-power RF plasma drives often employ TMNs based on mechanically adjusting physical passive components, such as by using stepper-motor-adjusted variable-vacuum capacitors [18]. While widespread, this technique is extraordinarily slow. Faster response can be obtained by appropriately adjusting bias conditions of electronic components such as varactors [8] or MEMS-varactors [9]. Nevertheless, power handling with such components is somewhat limited by the relatively high bias voltages required when operating at high power levels [10]. In digital TMNs, on the other hand, tunability is achieved by implementing the variable reactive elements as digitally-switched arrays, thus allowing adjustment of the impedance of the variable reactances in discrete steps. The realization of digital TMNs is typically based on CMOS switches [13], MEMS switches [11], PIN diodes [12] or discrete power transistors. MEMS switches are characterized with very low on-state resistance and can operate up to tens of GHz with negligible power consumption. The reliability of MEMS switch-based TMNs, however, is still an issue due to the large control voltages required by MEMS switches. On the other hand, PIN diode and CMOS switch-based TMN realizations offer the capability to handle very high power levels at the expense of some power loss in the switches due to their on-state resistance. Such TMN realizations are particularly favorable for on-die integration. The main drawback of digital TMNs, however, is their limited tuning resolution, and hence, the accuracy with which impedance matching can be achieved with an acceptable number of switched components. In some high power applications where accurate impedance matching is required over a very wide impedance range, such as RF plasma drivers, for example, the use of digital TMNs may be impractical due to the large number of digital switches needed to achieve the required fine tuning resolution. For instance, conventional high-power RF plasma drivers often still employ automatic antenna tuners based on stepper motor-adjusted continuously-variable capacitors as a result of the high requirements for accurate impedance matching and operation over very wide impedance ranges.

The limitations of existing techniques motivates improvement of the capabilities of TMNs to provide more accurate and faster impedance matching (higher tuning bandwidth) over wider impedance range while simultaneously allowing operation at high power levels with minimum insertion loss. This is the goal of the new approach developed here. Section II introduces the concept of phase-switched impedance modulation, Section III describes implementation and control

techniques for a PSIM-based tunable matching network and presents the design of a prototype system operating at frequencies centered at 13.56 MHz and at power levels up to 150 W. Section IV examines the performance of the prototype PSIM-based matching system, and Section V concludes the paper.

II. PHASE-SWITCHED IMPEDANCE MODULATION

Phase-switched TMNs achieve tunability by incorporating one or more phase-switched variable reactances. A phase-switched variable reactance modulates the effective impedance of a switched reactive element (capacitor, inductor, or some combination of both) by switching the connection of the element at the RF frequency. In essence, it is a narrow-band technique for controlling the effective impedance seen looking into the terminals of a reactive element at the frequency at which this element is switched (e.g., with a shunt or a series switch) by appropriately adjusting the phase and/or duty-cycle of the switch. The use of switched reactive elements was exploited in [14] in the different context of controlling resonant dc-dc converters by modulating their effective tank network resonant frequency, in [16] to tune the resonant frequency of a wireless power transfer receiver to a fixed transmitter frequency, and in to tune the tank network resonant frequency of a wireless power transmitter. However, it has not previously been applied to the notion of tunable matching networks for dynamic impedance matching.

To illustrate the notion of a phase-switched variable reactance, consider the parallel combination of a capacitor C_0 and an ideal switch being driven with a purely sinusoidal current source (see Fig. 1).

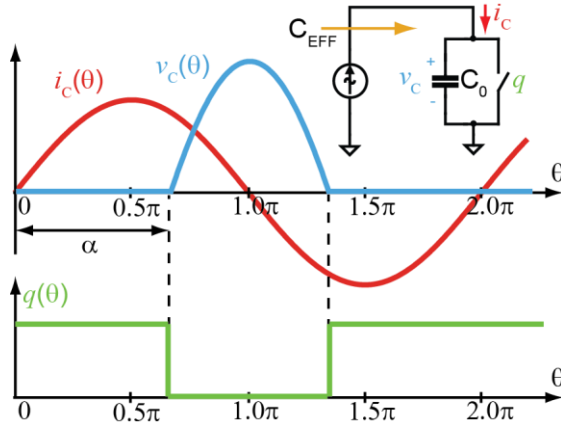


Fig. 1: Schematic illustrating the implementation of a phase-switched variable capacitance and its current and voltage waveforms. The effective capacitance C_{EFF} at the switching frequency can be modulated by controlling the conduction angle of the switch which is related to α .

The switch state is controlled by the signal q ; the switch is on or off when q is high or low respectively. If q is zero all the time, i.e. the switch is permanently turned off, then the effective capacitance C_{EFF} seen looking into the network is equivalent to the physical capacitance C_0 . On the other hand, if the switch is always on, then the capacitor C_0 is effectively shorted, and the network behaves as an infinite capacitor in the sense that the voltage across it remains zero irrespective of its terminal current (at the drive frequency). Thus it makes sense to conclude that

one ought to be able to control the effective capacitance C_{EFF} of the switched capacitor anywhere from C_0 to infinity by respectively controlling the conduction angle of the switch over the ac cycle from 0 to 2π .

Now suppose that the switch is turned off every cycle of the current waveform α radians after the current transitions from negative to positive, i.e. the switch is turned on α radians into the positive cycle of the current waveform (see Fig. 1), and it is turned back on after the capacitor voltage rings down to zero. The source current i_c , capacitor voltage v_c and switch control signal q for this scenario are shown in Fig. 1 as function of the cycle angle θ . Note that turning the switch on after the capacitor voltage rings down to zero ensures zero-voltage-switching (ZVS) turn on of the switch. Likewise, the switch turns off under ZVS owing to the capacitor C_0 in parallel with the switch, and C_0 naturally absorbs the parasitic switch capacitance. Each of these traits is valuable for efficient operation at high frequencies.

As can be inferred from Fig. 1, by adjusting α , i.e. setting how far into the cycle the switch turns on, one can control the conduction angle of the switch and hence, the voltage at which the capacitor peaks. It is clear from Fig. 1 that for a purely sinusoidal current source the conduction angle of the switch is given by 2α . Performing a harmonic analysis on the capacitor voltage (under sinusoidal current drive) reveals that its fundamental component lags the current by 90° for any switch conduction angle, suggesting that the switched capacitor network does indeed behave effectively as a variable capacitor at the switching frequency. Consequently, by analyzing the relationship between the switch conduction angle and the magnitude of the fundamental component of $v_c(\theta)$, it can be shown that the effective capacitance of the switched capacitor as a function of α is given by (1) [14].

$$C_{\text{EFF}} = \frac{\pi}{\pi - \alpha + \sin(\alpha) \cos(\alpha)} C_0 \quad (1)$$

Indeed (1) is consistent with the intuitive expectation for infinite effective capacitance when the switch is always in the on-state ($\alpha = \pi$) and predicts the equivalence between C_{EFF} and C_0 when the switch is permanently off ($\alpha = 0$). Fig. 2 plots the normalized effective capacitance C_{EFF}/C_0 of the switched-capacitor network of Fig. 1 at the switching frequency. As can be seen, C_{EFF} does indeed increase rapidly with α and approaches infinity with α approaching π (corresponding to a switch conduction angle of 2π).

The precision with which effective capacitance can be adjusted depends upon the resolution with which the switch conduction angle can be controlled. Although theoretically one can conclude that the effective capacitance can be modulated continuously over an infinite range, from a practical perspective, the range over which C_{EFF} can be modulated depends on the amount of harmonic distortion one is able to tolerate in the network.

As α increases towards π , the conduction angle (given by 2α for a purely-sinusoidal current excitation) of the switch increases, and hence the ringing of the capacitor voltage v_c (see Fig. 1) is limited to a shorter period. This results in significant harmonic content of the capacitor voltage for large C_{EFF}/C_0 ratios. The amount of harmonic distortion one can tolerate is

highly dependent on the limit of harmonic content that is allowed into the source and/or load. It is, however, important to distinguish between the harmonic distortion of the capacitor voltage of the switched network of Fig. 1 and the harmonic content that is actually injected into the source/load of the RF system. The switched network of Fig. 1 serves as a fundamental building block in the design of PSIM TMNs for RF systems; if necessary, additional filtering can be incorporated into these systems to further reduce injected harmonic content into the source and/or load.

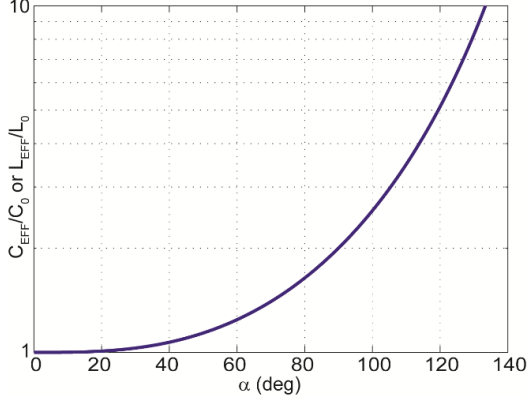


Fig. 2: Normalized effective capacitance C_{EFF} of the switched capacitor network at the switching frequency versus α for a purely sinusoidal current excitation.

The switched capacitor network serves as a fundamental building block for implementing phase-switched impedance modulation. This basic network is only able to provide strictly capacitive variable reactance (but not both). Nevertheless, some applications could benefit substantially from variable reactances whose value can be controlled over a range spanning both capacitive and inductive reactances, and/or by modulating the effective reactance over a more limited range. In such cases, one can further augment the basic capacitor switched network with additional reactive components to allow impedance modulation over a range that includes both capacitive and inductive impedances. It is further noted that one could also realize “full-wave” phase-switching reactance networks (having bidirectional voltages) and inductor-based phase-switched reactive networks, though for many RF applications the implementation of Fig. 1 is the most desirable approach.

III. TUNABLE IMPEDANCE MATCHING NETWORK IMPLEMENTATION

A. Network Design

To demonstrate the effectiveness of phase-switched impedance modulation for implementing tunable impedance matching, we utilize a TMN design based on an impedance step-up L-section matching network with electronically-variable effective impedances. Such a network configuration is particularly suitable for plasma applications (among others) where the drive-point impedance of an RF plasma-excitation coil must often be stepped-up and matched to the output impedance of a power amplifier (e.g., see [17] for a plasma matching system at similar power levels). As Fig. 4 shows, this network comprises input and output series resonant tanks along with a single phase-switched capacitor element.

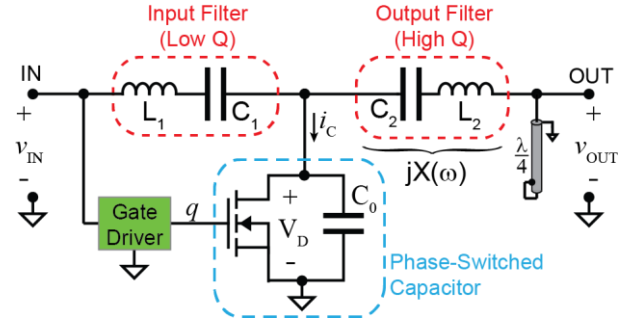


Fig. 4: Network topology of an L-TMN with dynamic-frequency tuning comprising a phase-switched capacitor C_0 and frequency-controlled reactance X . The input filter reactance does not vary considerably with frequency modulation.

It's important to recognize that in order for any TMN to be able to match load impedances that vary independently both in resistance and reactance (i.e. provide an impedance match over a two-dimensional region in the Smith chart), the TMN must comprise at least two reactances that can be tuned quasi-independently. In the case of the TMN of Fig. 4, one of the variable reactances is the shunt capacitance realized with the phase-switched capacitor C_0 . While we could implement the second variable reactance using another phase-switched capacitor, here we utilize a different technique. The second variable reactance is implemented using the series-resonant output tank formed by C_2 and L_2 : its reactance X is controlled by narrow-band frequency modulation about the nominal operating frequency. Thus the TMN design demonstrated here utilizes frequency modulation as a second control handle for load impedance transformation. Here we refer to this technique as dynamic-frequency tuning (DFT). The impedance jX of the output tank is determined by the characteristic impedance of the tank Z_0 and the deviation of the operating frequency f from the tank's resonant frequency f_0 and is given by (2).

$$X = Z_0 \frac{(f - f_0)^2}{f_0 f} \quad (2)$$

As (2) suggests, the range over which the output reactance X is adjustable can be expanded by either choosing L_2 and C_2 to obtain higher tank characteristic impedance, or by allowing for larger amounts of frequency modulation (or both). The amount of frequency modulation allowed is highly dependent on the particular application. In addition to serving as a frequency-variable tunable reactance, the L_2/C_2 tank also provides filtering, limiting the injection of high-frequency harmonic currents into the output. Similarly, the input filter comprising L_1 and C_1 is designed to be series-resonant at the nominal operating frequency thus limiting the injection of high-frequency harmonic content by the TMN back into the PA. The characteristic impedance of this input tank may be selected to be much smaller than that of the output tank to avoid significant variation of its reactance with frequency modulation.

Note that C_1 and C_2 in the system of Fig. 4 also serve as dc blocking capacitors providing dc isolation between the drain of the switch and the PA and load respectively. This is an important requirement for this TMN implementation since modulating the conduction angle of the switch imposes a variable dc bias of the drain which could interfere with the source or load. The shorted quarter-wavelength stub in parallel with the output of the TMN

in Fig. 4 serves to provide additional filtering of even harmonic components. It reduces harmonic content injected in the load by presenting a shunt impedance at the TMN's output that is high at odd harmonics and low at even harmonics of the operating frequency. For the design presented here, the impedance of the stub (at the fundamental frequency) is much larger than the load impedance over the entire load and frequency operating range of the TMN. Hence, besides the additional filtering it provides, the quarter-wavelength stub does not impact the control of the TMN, i.e. the choice of frequency and switch conduction angle for matching a load to the PA. Of course, depending on the particular application, one may adopt different output filter designs. The TMN design presented here is tailored towards driving plasma loads, and for the particular application it is desirable to keep the harmonic content injected in the output to less than -20 dBc.

The L-TMN prototype described here is designed to operate at a nominal frequency of 13.56 MHz in the ISM band with up to $\pm 10\%$ frequency modulation ($L_1 = 1.17 \mu\text{H}$, $C_1 = 117 \text{ pF}$, $L_2 = 2.97 \mu\text{H}$, $C_2 = 47.5 \text{ pF}$, $C_0 = 270 \text{ pF}$). The yellow-shaded and the dotted red-line regions in the Smith chart of Fig. 5 illustrate the range of load impedances that this TMN design can successfully match to a 50Ω source impedance for 5% and 10% frequency modulation respectively. (The frequency modulation percentage is defined here as the ratio of the peak frequency deviation to the nominal operating frequency.) As can be seen from Fig. 5, the range of reactive loads that the TMN can match to 50Ω increases with the amount of frequency modulation. Hence, for every particular value of load impedance within the tunable range, there is a unique combination of operating frequency and switch conduction angle α that is required to provide an impedance match between the load and the PA.

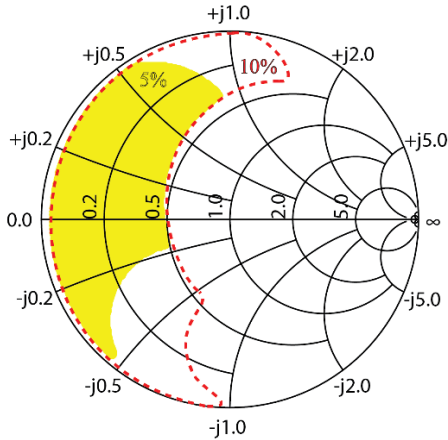


Fig. 5: Typical load impedance range that can be matched to a 50Ω source with 5 % (yellow) and 10 % (red) frequency modulation for the TMN design of Fig. 4 with $L_1 = 1.17 \mu\text{H}$, $C_1 = 117 \text{ pF}$, $L_2 = 2.97 \mu\text{H}$, $C_2 = 47.5 \text{ pF}$, $C_0 = 270 \text{ pF}$.

The load impedance ranges shown in Fig. 5 correspond to modulating the effective capacitance of the RF-switched capacitor by up to 4X the value of the base capacitance C_0 . (Such amount of capacitance modulation roughly corresponds to varying α in Fig. 1 from 0° to 110° .) Further capacitance modulation expands the TMN matching range (at the expense of injecting higher harmonic content into the load and the PA) to

include load impedances with lower resistive components. On the other hand, decreasing the base capacitance C_0 (while allowing the same amount of capacitance modulation) results in shifting the TMN matching range towards load impedances with higher resistive components. Note that with the network topology shown in Fig 1, one can conveniently use C_0 to absorb the drain-to-source capacitance of the switch (and in particularly high-frequency implementations, C_0 may comprise only switch capacitance).

To illustrate the operation and control of the TMN design of Fig. 4 in more detail, consider the Smith chart (see Fig. 6) with some inductive and capacitive loads Z_1 and Z_2 respectively that one wishes to match to 50Ω (the center of the Smith chart). The dashed circle corresponds to a conductance of 0.2 S , i.e. the equivalent load of a 50Ω resistance in parallel with some reactance.

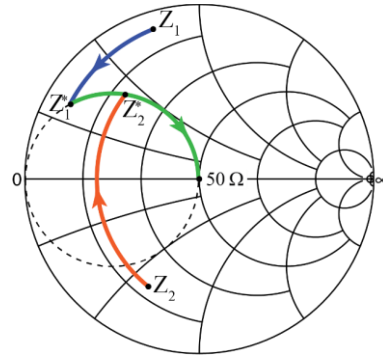


Fig. 6: Impedance matching of an inductive load Z_1 and capacitive load Z_2 using the TMN of Fig. 4 by first performing frequency control and then phase-switched capacitance modulation.

For the L-section matching network design of Fig. 4, frequency modulation causes the TMN's input impedance to move along a circle of constant resistance in the Smith chart (e.g., red and blue curves in Fig. 6). On the other hand, phase-switched capacitance modulation results in the TMN's input impedance traversing a circle of constant conductance in the Smith chart (green curve in Fig. 6). (Here we ignore the small effect of the input filter on the TMN's input impedance with frequency modulation.) Thus, in the context of the TMN design presented here, one can visualize the mechanism of impedance matching as a two-step process consisting of frequency control followed by switched-capacitance modulation. For example, in the case of matching load Z_1 in Fig. 6, one can first begin by decreasing the operating frequency below the resonant frequency f_0 of the output tank so as capacitively offset the load and thus bring the TMN's input impedance to the point Z_1^* on the 0.2 S dashed conductance circle (blue line). At this point, one can proceed by increasing the conduction angle of the switch, forcing the TMN's input impedance to traverse along the dashed conductance circle until it reaches 50Ω (green line). This essentially corresponds to adjusting the effective shunt capacitance to resonate out the susceptive component of Z_1^* . On the other hand, when matching a capacitive load such as Z_2 , one may begin by first increasing the frequency above f_0 to inductively offset the load to point Z_2^* on the 0.2 S conductance circle (orange line) and then appropriately increase switch conduction angle until the TMN's input impedance reaches 50Ω (green line). As Fig. 6 suggests, loads with larger resistive

components require less shunt capacitance, and hence, a smaller switch conduction angle. In terms of frequency control, inductive loads require smaller operating frequency than capacitive loads. Note that one can reactively offset the entire TMN matching range shown in Fig. 5 by simply changing the resonant frequency of the output tank.

B. Gate-Waveform Generation and Synchronization

The ability to synthesize the appropriate gate waveform for driving the switch is of crucial importance to the TMN operation. As Fig. 1 suggests, the gate drive signal q should be synchronized to the current i_C flowing through the switched-capacitor network over the entire TMN frequency modulation range. Furthermore, one must be able to accurately control the conduction angle of the switch. In essence, this requires one to generate a gate waveform with a variable duty cycle synchronized to the switched capacitor current i_C . The resolution with which one can vary the duty cycle determines the resolution with which the effective capacitance can be modulated and hence sets the limit on the overall TMN impedance matching resolution. Synchronizing the gate drive signal directly to the switched-capacitor current waveform, however, can be problematic as this requires one to measure the current i_C ; measurement of RF current waveforms is often a challenge. Instead, for the TMN design presented here, we offer an alternative approach based on synchronizing the gate drive signal q with the TMN's input voltage v_{IN} .

To illustrate this approach, consider the TMN design presented in Fig. 4. Since the TMN's input filter is series-resonant at the 13.56 MHz nominal operating frequency, the fundamental frequency components of v_{IN} and the drain voltage v_D are in phase at this frequency. Furthermore, since the phase-switched capacitor network behaves effectively as a capacitor, the fundamental frequency component of the switched capacitor current i_C leads that of v_D by 90° . Of course, this is exactly true only at the nominal operating frequency – the frequency at which the TMN's input filter is series-resonant. However, in the prototype design considered here, the characteristic impedance of the input filter is selected to be relatively low compared to $50\ \Omega$, and as a result, the filter remains nearly-resonant over the entire frequency modulation range. It can be shown that for the TMN design of Fig. 4, the phase shift between the fundamental components of v_{IN} and i_C is approximately $90^\circ \pm 5^\circ$ over the full 10% frequency modulation range and the corresponding load impedance range shown in Fig. 5. Hence, by synchronizing the gate drive signal directly to the TMN's input voltage (and by appropriately phase-shifting it), one is able to effectively synchronize the switching of the capacitor to the current i_C . This is the underlying principle of the proposed gate-drive synchronization approach.

As Fig. 7 illustrates in more detail, the gate-drive signal q having variable pulse width w is phase-locked to the TMN's input voltage v_{IN} , i.e. a phase shift Φ is maintained between the rising edge of q and the negative-to-positive v_{IN} transition. As we discuss shortly, the gate drive signal generation circuit is capable of independently controlling both Φ and w over the entire frequency modulation range. Since i_C leads v_{IN} by approximately 90° , one can choose w and Φ appropriately so that the switch is turned on for a duration α ($0 \leq \alpha \leq \pi$) after the

negative-to-positive transition in i_C . Note that if the switch is not turned on immediately after the drain voltage v_D rings back down to zero, since at this instant the current i_C is negative, the switch goes into reverse conduction mode and the body diode clamps the drain voltage near zero. Assuming the switched capacitor current i_C in Fig. 7 is purely sinusoidal, it can be shown that the duration of the reverse conduction mode is also α . To ensure zero-voltage switching (ZVS), the switch must be turned on either exactly at the negative-to-positive transition of i_C , or while the body-diode is conducting. Of course, in the latter case, the phase shift Φ between q and v_{IN} must be appropriately selected with the pulse width w chosen greater than α . This allows one to use the body-diode conduction mode effectively as a ZVS safety margin by alleviating the requirement for precise switch turn-on; ZVS operation is guaranteed, provided that the switch is turned on anytime during the body-diode conduction mode.

It is important to clarify that although the gate driving circuit is capable of generating a signal q with arbitrary pulse width w and phase shift Φ which are unaffected by frequency modulation, this is not the case for the forward conduction angle α , i.e. a constant pulse-width and phase of q does not imply a constant α as the TMN's operating frequency is modulated. This is because the gate drive signal q is phase-locked with respect to v_{IN} , and hence, any small variation in the phase shift between the fundamental components of i_C and v_{IN} translates directly into modulation of forward conduction angle α of the switch. Similarly, this also affects the duration of the reverse conduction mode. For instance, if the phase shift between v_C and i_C changes by Δ from the nominal 90° (e.g., due to modulation of the operating frequency), the switch will stay in forward conduction mode for a duration of $\alpha + \Delta$ assuming phase Φ and pulse width w of the gate drive signal q are kept constant.

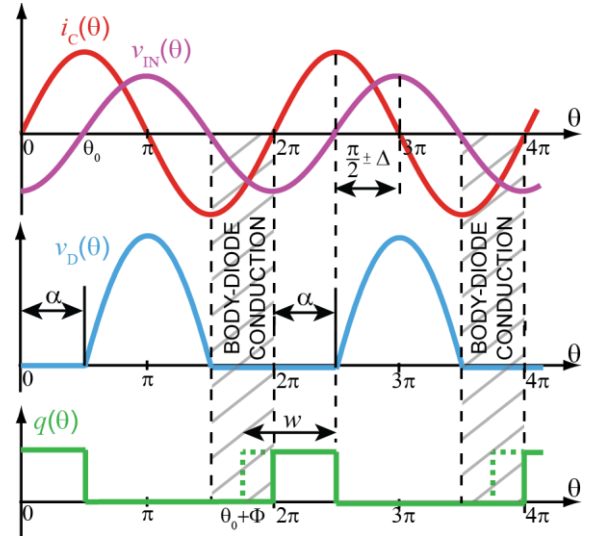


Fig. 7: Current and voltage waveforms for the TMN of Fig. 4. The switch gate waveform q is phase-locked with respect to the TMN input voltage v_{IN} , which is lagging the current through the switched-capacitor network i_C by approximately 90° . By controlling the switch conduction angle one can adjust the effective capacitance of the switched capacitor.

Control of the switch forward conduction α and the TMN's operating frequency is the responsibility of an external feedback loop. For example, such a feedback loop could be based on

monitoring the quality of impedance matching between the power amplifier and the TMN by measuring the reflected power or the impedance at the TMN's input port. (The design of a high-bandwidth feedback control loop for this purpose will be the subject of future work.) Of course, to guarantee zero voltage switching over the entire TMN operation range, Φ must be chosen appropriately to allow for variation in the phase shift between v_{IN} and i_C as frequency is modulated.

To do so, one can begin by first estimating the expected variation Δ in the 90° nominal phase shift between i_C and v_{IN} for a given TMN frequency and load operating range. Then, by selecting a minimum bound α_{min} on the switch forward conduction angle such that $\alpha_{min} > 2\Delta$ under nominal conditions (v_{IN} lags i_C by 90°) one also guarantees a switch reverse conduction period (with v_D being clamped to approximately 0 V) of at least α_{min} (under nominal conditions). Since the phase between i_C and v_{IN} can decrease by at most Δ , the width of the reverse conduction remains always greater than $\alpha_{min} - \Delta = \Delta$ over the entire TMN operating range. By ensuring that the switch is turned on only during the reverse conduction mode, ZVS operation is guaranteed. This can easily be achieved by selecting the phase Φ of q such that its rising edge occurs half-way across the reverse conduction mode of the switch under nominal conditions as shown in Fig. 7 by the dotted edge, i.e. $\Phi = 3\pi/2 - \alpha_{min}/2$. Maintaining this constant phase shift between v_{IN} and q while limiting the minimum pulse width to $w_{min} = 3\alpha_{min}/2$ ensures ZVS over the full frequency modulation range. For example, in the TMN design presented here, as we already mentioned, the maximum variation Δ in the phase shift between i_C and v_{IN} is approximately 5° . Thus, we can choose $\alpha_{min} = 20^\circ$ resulting in $\Phi = 260^\circ$ and a minimum allowed gate signal pulse width of 30° .

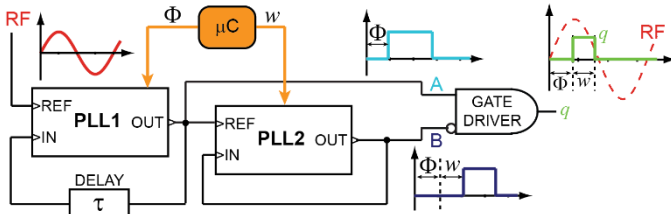


Fig. 8: Block diagram of the gate driver circuit employed for generating a variable duty-cycle waveform with pulse width w and phase shift Φ . The time delay element τ in the feedback path of PLL1 is selected to match the gate driver delay and thus eliminate the dependence of Φ on frequency modulation.

Here we introduce a PLL-based approach for generating a variable duty cycle gate waveform that allows one to control its pulse width w and phasing Φ (relative to an input voltage) independently from frequency, i.e. frequency modulation affects neither w or Φ . This greatly simplifies the overall system control. (The ability to dynamically control Φ is not necessary for the operation of the TMN design presented here; it is incorporated in the design of this gate driver only for additional versatility.) The gate driver circuit comprises a cascade of two PLL modules (see Fig. 8). Each PLL module is designed to generate an output signal at its OUT terminal such that the signal fed back to its IN terminal is frequency-locked to the reference signal at its REF terminal and is phase-shifted from it by a certain amount. This phase shift is digitally controlled by a microcontroller and can be adjusted from -180° to 180° with a

10-bit resolution. The resolution is a result of the particular implementation of the PLL and can be easily increased.

Consider Fig. 8 and assume for a moment that the time delay element in the feedback path of PLL1 is zero. This causes PLL1's output signal A to be frequency-locked to the RF input and phase-shifted from it by Φ . For the particular implementation of PLL1, a phase shift of Φ between the reference and the output signals implies that the rising edge of the output signal pulse lags the negative-to-positive transition in the reference signal by Φ . In turn, the output of PLL1 serves as the input of PLL2, whose output signal B is phase-shifted by w from signal A (See Fig. 8). Signals A and B are combined through gate drive logic to produce the signal q with variable pulse width w and phase shift Φ between its rising edge and the negative-to-positive transition of the RF signal. Note that by selecting the time delay τ in the feedback path of PLL1 to match the delay of the gate driver, one can eliminate the dependence on frequency of the phase shift between q and the RF signal. In the TMN design presented here, the RF reference signal fed to PLL1 is obtained directly from the TMN's input voltage v_{IN} (see Fig. 4) through capacitive voltage division.

The gate-waveform generation module of Fig 8 is capable of generating a variable duty-cycle gate drive which can be adjusted from 0 % to 100 % with 0.1 % resolution while synchronizing it to the switched-capacitor current waveform over the entire frequency modulation range. As mentioned, this resolution in duty-cycle control is a result of the particular implementation and can be easily increased if it need be.

C. System Implementation

One can think of the TMN system proposed here as comprising a power stage and a gate-waveform generation module. The power stage consists of the RF phase-switched capacitor and the input and output filters as shown in Fig. 4, and it is responsible for providing the load-to-source impedance match. A 650 V GaN FET (GS66508, GaN Systems) is used for a switch due to its fast turn-on and turn-off times and relatively low output device capacitance (65 pF at 400 V drain-to-source voltage). The device capacitance forms the entire phase-switched capacitor C_0 . Both inductors are coreless solenoids with a 3" inside diameter and wound with 0.25" copper tube (see Fig. 9).

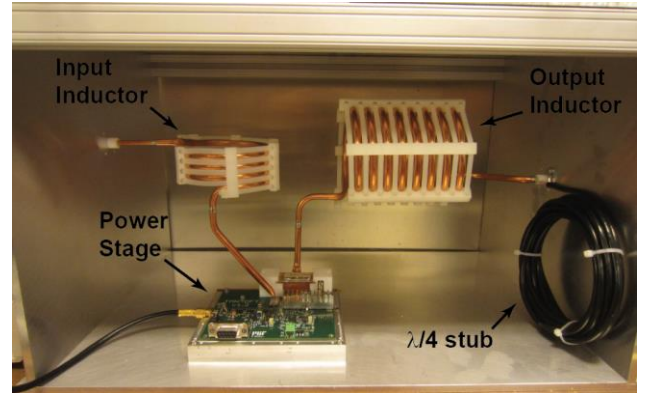


Fig. 9: Overall TMN system implementation showing the input and output filter inductors, the power stage and the quarter-wavelength stub.

The input filter inductor L_1 comprises 3.75 turns approximately 0.55" turn-to-turn spacing plus interconnect. Its inductance is measured to be approximately 1.2 μH with a quality factor greater than 900 at 13.56 MHz. The output filter inductor is wound with 8 turns with approximately 0.51" turn-to-turn spacing plus interconnect and has a measured inductance of 3.2 μH and a quality factor of approximately 800 at 13.56 MHz. Machined delrin spacers are fitted between the turns of the inductors for a more rigid construction. The resonant frequency of the input and output filters is tuned to be respectively 13.56 MHz and 13.40 MHz by adjusting the values of the input and output filter capacitors C_1 and C_2 . C_1 has a total capacitance of approximately 115 pF and is formed by the parallel combination of 1.5 kV NP0 ceramic capacitors (HIFREQ series, Vishay), while C_2 consists of a series-parallel combination of 2.5 kV NP0 ceramic capacitors (HiQ series, AVX) with a total capacitance of approximately 44 pF. The quarter-wavelength stub at the TMN's output is made of approximately 3.65 m of 50 Ω coax cable (RG58) coiled and shorted at one end. The TMN implementation presented here is rated up to 200 W of RF input power. The power stage and the gate-waveform generation module are integrated onto a single 4-layer FR4 PCB (see Fig. 10).

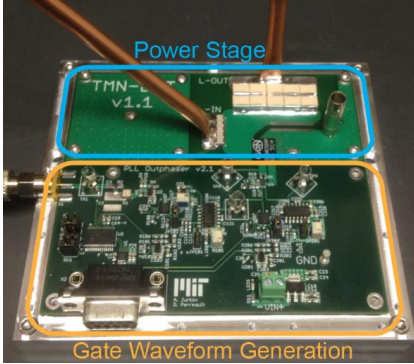


Fig. 10: Closer view of the power stage along with the gate waveform generation module. Control of the switch conduction angle is achieved through a UART serial interface.

IV. EXPERIMENTAL PERFORMANCE

A. Measurement Setup

To evaluate the performance of the matching system presented here, the TMN is powered from a 150 W RF power amplifier (150A100B, Amplifier Research) having a 50 Ω output impedance as shown in Fig. 11. It is sinusoidally excited by a function generator (DG2041A, Rigol) whose frequency can be externally adjusted. The power amplifier is connected to the TMN through an I-V probe (Model#: 000-1106-117, MKS Instruments) which directly measures the input impedance looking into the TMN. The TMN's output port is terminated with a resistive/reactive load impedance located within the 10 % frequency-modulation matching range shown in Fig. 5.

To test the TMN, we utilize a home-built adjustable RF load. To facilitate ease of adjustment of the load over the targeted impedance range, the load is implemented with a variable length transmission line (50 Ω RG214 coax cable) terminated with the parallel combination of a 50 Ω RF power resistor (CTN-250-2, Meca Electronics Inc.) and a variable vacuum capacitor

(CVMN-1000A, Comet). By adjusting the length of the line from 0 to 3 m and varying the capacitance over a 50 pF – 1000 pF range allows one to generate all the inductive loads and most of the capacitive loads in Fig. 5 corresponding to the 5 % frequency modulation load range.

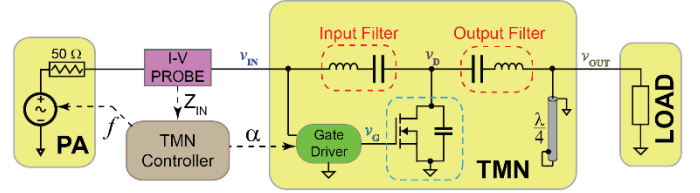


Fig. 11: Experimental setup for measuring the performance of the TMN. The switch conduction angle α and the operating frequency f are adjusted until the load is matched to 50 Ω . The TMN's input impedance is measured directly by an I-V probe.

B. TMN Performance

To demonstrate the performance of the TMN, the switch conduction angle and the operating frequency are adjusted until the I-V probe measures 50 Ω input impedance, i.e. the load is matched to the power amplifier.

TABLE I. SWITCH CONDUCTION ANGLE AND TMN OPERATION FREQUENCY REQUIRED TO MATCH VARIOUS LOAD IMPEDANCES TO A 50 Ω SOURCE IMPEDANCE.

Test Case	Load (Ω)	Conduction Angle ($^\circ$)	Frequency (MHz)
A	$19.1 + j32.3$	0	13.18
B	$20.3 + j1.62$	0	13.99
C	$17.9 - j13.6$	144.8	14.37
D	$9.91 + j24.7$	182.8	13.36
E	$9.61 - j1.10$	195.1	13.97
F	$10.0 - j16.3$	194.6	14.38
G	$5.40 + j31.6$	210.6	13.06
H	$3.97 + j0.98$	218.8	13.81
K	$5.33 - j11.8$	206.2	14.18

Table I shows example of load impedances (along with the required switch conduction angle and operating frequency) at which the TMN matches the load to 50 Ω at 150 W power output from the PA with less than 1 % of reflected power at the input port of the TMN. Note that the conduction angle in Table I reflects the total switch conduction angle, i.e. it is the combination of forward and reverse device conduction. As can be seen, the TMN is able to match a wide range of capacitive and inductive loads as suggested by Fig. 5. Consistent with the expected operation of the L-section-based TMN design, matching of loads with small resistive components requires larger switch conduction angles. As the resistive component of the load increases, the required conduction angle decreases. In terms of frequency control, the larger the inductive component of the load, the smaller the frequency required to provide impedance matching, while loads with larger capacitive components demand higher operating frequency, as expected.

An example oscilloscope snapshot of the TMN voltage waveforms at the input port v_{IN} , output port v_{OUT} , switch drain v_D , and the gate-drive v_G for a $5.00 + j15.6 \Omega$ inductive load (test

case G, Table I) at 150 W of input power (into the TMN) is shown in Fig. 12. It can be clearly seen that the switch exhibits zero-voltage turn-on which is a highly desired feature for reducing switching losses. Note that for the test case illustrated in Fig. 12, the drain voltage rings down to zero and stays near 0 V even before the switch is commanded to turn on due to reverse switch conduction. In addition, Fig. 12 shows a nearly-pure sinusoidal TMN output voltage (the voltage across the load) suggesting a relatively small harmonic content injected into the load (measured to be less than -20 dBc). Similar output harmonic content is found for the rest of the test cases in Table I. On the other hand, one can easily notice that the input TMN voltage has significant harmonic content for the test case in Fig. 12. A small portion of it is due to relatively weak input filtering of the drain voltage. However, most of the harmonic content observed in TMN input voltage is attributed to near-saturation of the power amplifier used to drive the TMN. Similar voltage waveforms are measured for the rest of the test cases in Table I suggesting that the PSIM-based TMN implementation proposed here is effective at accurately matching a wide range of load impedances.

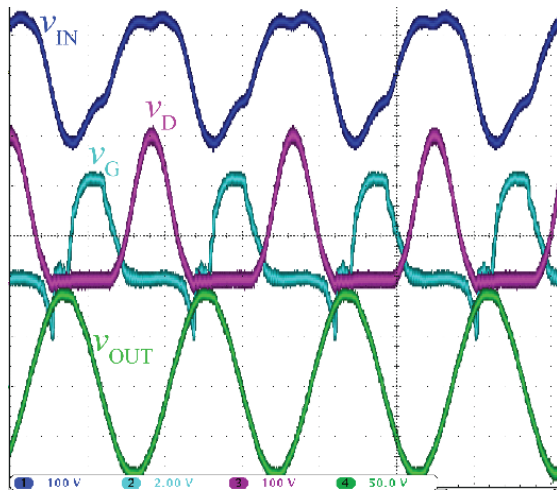


Fig. 12: TMN input port voltage v_{IN} , output port voltage v_{OUT} , gate-drive voltage v_G and switch drain-to-source voltage v_D for test case G (Table I) at 150 W of RF input power into the TMN.

V. CONCLUSION

This work proposes a tunable matching network based on *phase-switched impedance modulation* (PSIM), a technique for implementing variable impedances based on switching of passive elements at the RF operating frequency. We introduce a PSIM impedance and matching network implementation that enables zero-voltage-switching of the active device with simple timing. Moreover, we introduce a PLL-based modulation control system that provides the necessary sensing and drive of the PSIM circuit. To demonstrate the effectiveness of the proposed approach we present a PSIM-based TMN design capable of matching a wide load impedance range associated with inductively-coupled plasma processes to a 50 Ω power amplifier. The TMN's performance is demonstrated in a narrow frequency band centered around 13.56 MHz at an input RF power of up to 150 W. The matching network presented here provides accurate impedance matching (to < 1% reflected power) while injecting less than -20 dBc of harmonic content in

the load and maintaining zero-voltage-switching over the entire load range. Such a PSIM-based TMN opens the door to a combination of much faster and more accurate impedance matching than is available with conventional techniques, and is suitable for use at high power levels.

REFERENCES

- [1] J. Mitola, "The software radio architecture," *IEEE Communications Magazine*, Vol. 33, No. 5, pp. 26-38, May 1995.
- [2] Nemati, et. al., "Design of Varactor-based tunable matching networks for dynamic load modulation of high power amplifiers," *IEEE Transactions on Microwave Theory and Techniques*, Vol. 57, No. 5, pp. 1110-1118, May 2009.
- [3] R. Malmqvist, et. al., "RF MEMS based impedance matching networks for tunable multi-band microwave low noise amplifiers," in *Proc. 2009 International Semiconductor Conference*, Vol. 1, pp. 303-306.
- [4] S. Nagarkatti, et. al., "Radio frequency power delivery system," U. S. Patent 8 633 782, Jan. 21, 2014.
- [5] G. J. J. Winands, et. al., "Matching a pulsed power modulator to a corona plasma reactor," *2007 IEEE International Pulsed Power Conference*, pp. 587-590, June 2007.
- [6] D. Goodman, et. al., "RF power supply with integrated matching network," U.S. Patent 6 887 339, May 3, 2005.
- [7] Y. Lim, et. al., "An adaptive impedance-matching network based on a novel capacitor matrix for wireless power transfer," *IEEE Transactions on Power Electronics*, Vol. 29, No. 8, pp. 4403-4413, Aug. 2014.
- [8] W. C. E. Neo, et. al., "Adaptive multi-band multi-mode power amplifier using integrated Varactor-based tunable matching networks," *IEEE Journal of Solid-State Circuits*, Vol. 41, No. 9, pp. 2166-2176, Sep. 2006.
- [9] Q. Shen and N. S. Barker, "Distributed MEMS tunable matching network using minimal-contact RF-MEMS varactors," *IEEE Transactions on Microwave Theory and Technology*, Vol. 54, No. 6, pp. 2646-2658, Jun. 2006.
- [10] M. T. Arnous, Z. Zhang, S. E. Barbin and G. Boeck, "Characterization of high voltage varactors for load modulation of GaN-HEMT power amplifier," *2015 17th International Conference on Transparent Optical Networks (ICTON)*, Budapest, 2015, pp. 1-4.
- [11] A. van Bezooijen, et. al., "A GSM/EDGE/WCDMA adaptive series-LC matching network using RF-MEMS switches," *IEEE Journal of Solid-State Circuits*, Vol. 43, No. 10, pp. 2259-2268, Oct. 2008.
- [12] C. Sanchez-Perez, et. al., "Design and applications of a 300-800 MHz tunable matching network," *IEEE Journal on Emerging and Selected Topics in Circuits and Systems*, Vol. 3, No. 4, Dec. 2013.
- [13] P. Sjöblom and H. Sjöland, "Measured CMOS switched high-quality capacitors in a reconfigurable matching network," *IEEE Transactions on Circuits and Systems II*, Vol. 54, No. 10, pp. 858-862, Oct. 2007.
- [14] W. Gu, and K. Harada, "A new method to regulate resonant converters," *IEEE Transactions on Power Electronics*, Vol. 3, No. 4, Oct. 1988.
- [15] F. C. W. Po, E. de Foucauld, D. Morche, P. Vincent, and E. Kherherve, "A novel method for synthesizing an automatic matching network and its control unit," *IEEE Transactions on Circuits and Systems – I*, Vol. 58, No. 9, pp. 2225-2236, Sept. 2011.
- [16] E. Waffenschmidt, "Dynamic resonant matching method for a wireless power transmission receiver," *IEEE Transactions on Power Electronics*, Nov. 2015, pp. 6070-6077.
- [17] A. Al Bastami, et. al., "Dynamic matching system for radio-frequency plasma generation," *2016 IEEE Energy Conversion Congress and Exposition*, Milwaukee, WI, 2016, pp. 1-7.
- [18] G. Bacelli, J. V. Ringwood, and P. Iordanov, "Impedance matching controller for an inductively coupled plasma chamber: L-type matching network automatic controller," *4th International Conference on Information in Control, Automation and Robotics*, Angers, France, 2007.
- [19] J. Tian, and A. P. Hu, "A DC-voltage-controlled variable capacitor for stabilizing the ZVS frequency of resonant converters for wireless power transfer," *IEEE Transactions on Power Electronics*, Vol. 32, No. 3, pp. 2312-2318, March 2017.